

# DSMC Computations of Leading-Edge Separation in Hypersonic Flows

Ram Prakash<sup>\*†</sup>, Sudhir Gai<sup>\*</sup> and Sean O'Byrne<sup>\*</sup>

<sup>\*</sup>UNSW - Canberra

School of Engineering & IT, UNSW - Canberra, ACT 2610, Australia.

ram.prakash@student.adfa.edu.au · s.gai@adfa.edu.au · s.obyrne@adfa.edu.au

<sup>†</sup>Corresponding author

## Abstract

A leading-edge separation model is computationally studied to investigate the separation and re-attachment characteristics using the DSMC code SPARTA. The computational challenges in obtaining meaningful DSMC results in flows close to continuum is presented through extensive convergence studies. When the flow domain spans different regimes, from transitional to continuum, the local flow as well as grid based Knudsen number can be a suitable adaptation criterion for grid refinement. Though the quality of convergence is checked mainly through the separation length of the primary vortex, the peak values of surface parameters and the secondary vortex length are also evaluated. However, any significant changes in the flow structure over a longer time can have a detrimental effect on such flow adapted grids unless either a continuous adaptation is chosen or at least the adaptation procedure is carried out at set frequent steps. The salient features of separation and re-attachment at 1.25ms flow time show a distinct primary vortex and a developing secondary vortex at the corner. The primary separated region can be clearly identified in the shear stress and velocity slip distributions but the secondary structure is not well resolved. A theoretical evaluation of streamline angles at separation and re-attachment, based on Oswatitsch's relationship, shows that the streamline behavior agrees well with the slip corrected expression of this relationship.

## 1. Introduction

The leading-edge separation model was first proposed by Chapman et al,<sup>1</sup> based on a limiting case for separation in the widely studied compression corner and rearward facing step models. A leading edge separation is less complicated for analytical investigation due to the absence of a developed boundary layer at the onset of separation so that the requirement for a boundary layer analysis is eliminated. With this model, Chapman proposed a theoretical relation between dead air pressure in the separated region and the static pressure after re-attachment. The experimental studies to verify this relation were conducted in the supersonic range, which was the need of the time. In hypersonic flows, there have been studies done on separation using generic models such as compression corners,<sup>2</sup> rearward facing steps,<sup>3</sup> hollow cylinder flares and biconic shapes<sup>4</sup> etc. However, all these generic models are characterized by the existence of a finite thickness boundary layer prior to separation. There is still a dearth of literature when it comes to leading edge separation studies in hypersonic flows. The objective of the present study is to abridge that gap, with a Direct Simulation Monte Carlo (DSMC) computational investigation being done on a 'tick' shaped model that promotes leading edge separation.

Recently, the leading-edge separation problem in hypersonic flows has generated a reignited curiosity among the research world. Many researchers, over the last few years, have contributed towards DSMC based computational investigation of separation characteristics associated with a 'tick' model, starting with the studies performed by Moss et al<sup>5,6</sup> using the DS2V code.<sup>7</sup> The present authors also performed similar studies on this configuration using DS2V,<sup>8</sup> with detailed inferences made on slip behavior and incipient separation. Further to this, another study<sup>9</sup> by the present authors highlighted the code-to-code comparison with DS2V and SPARTA on the same model. More recently, the present authors<sup>10</sup> have presented a detailed study on separation characteristics of high enthalpy, low density flow over the model along with discussions on the effects of leading-edge bluntness and surface accommodation coefficients. The flow conditions employed in all the above studies are based on the ongoing high enthalpy experiments (designated as Condition A2) at T-ADFA free-piston shock tunnel.<sup>11</sup> The focus of the present work is on a relatively low enthalpy, high density condition, designated as Condition E, which again is part of the experimental program at the same facility.

## LEADING-EDGE SEPARATION

Some initial DSMC computations are performed by Tumuklu et al<sup>12</sup> for this condition, using the code SMILE, and results presented in their work are used for comparison here.

The flow configuration over the ‘tick’ model and the computational geometry are explained briefly in section 2 along with free-stream flow conditions. Thereafter, the convergence studies carried out to minimize the statistical and discretization errors are explained in section 3. The primary features of flow separation are described in section 4 for a sharp leading edge case. The surface parameters are presented in terms of non-dimensional coefficients of heat flux ( $C_h$ ), skin friction ( $C_f$ ), pressure ( $C_p$ ) and absolute values of velocity slip ( $V_{slip}$ ) and temperature jump ( $T_{jump}$ ). The theoretical analysis of streamline angles at separation and re-attachment on the basis of Oswatitsch’s relationship<sup>13</sup> are discussed in section 5. Finally some conclusions are drawn out in section 6.

## 2. ‘Tick’ configuration and free-stream conditions

The flow schematic and the computational model used for flow analysis are shown in Fig.1. It is a generic schematic, in which the separation location (B) can occur anywhere on the expansion surface between the leading-edge (A) and the corner (C). For a leading-edge separation, B would be located very close to A. The onset of separation is dictated by the balance between the expansion process at the leading-edge and adverse pressure gradient from the corner. For a low enthalpy, high density free-stream condition, the expansion is relatively weaker in comparison to a high enthalpy, low density free-stream. Therefore, the adverse pressure effect is felt further upstream and the flow separation occurs very close to A, resulting in a leading-edge separation. In such situations, separation and leading-edge shocks merge within a few distance downstream and propagate further down as a single shock. The separated shear layer eventually re-attaches at D, somewhere along the compression surface CE. Though the separated re-circulation region (BCD) is shown as a single vortex structure, there might be possibilities of secondary vortex structures due to local interaction between the surface and the primary vortex. In addition, in any corner induced separated flow, there is always the presence of a small corner eddie, known as Moffat eddie,<sup>14</sup> when the included corner angle is  $\leq 146$ deg. The expansion waves, emanating from the triple point results in a sharp reduction of the peak values of surface properties that normally occur along the neck region at the start of the re-compression shock.

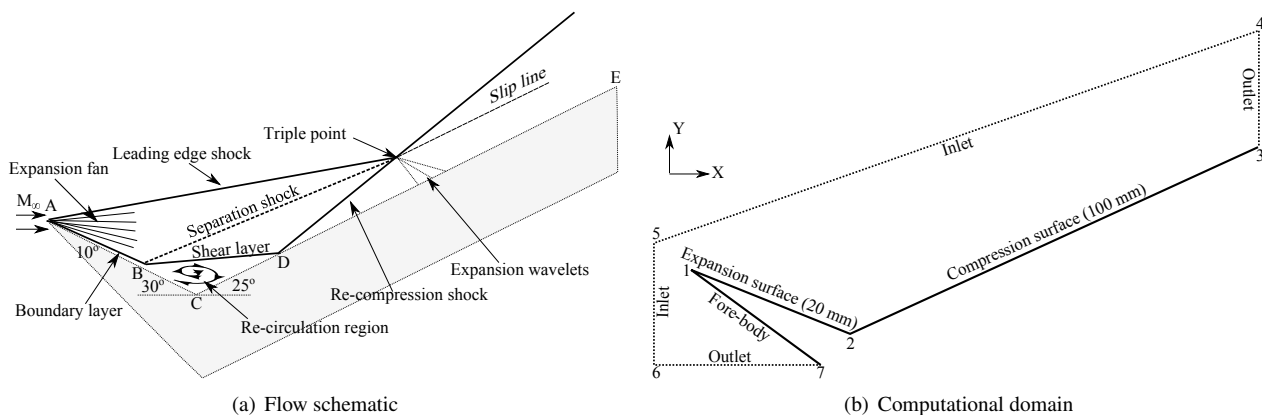


Figure 1: ‘Tick’ configuration

The free-stream flow conditions are based on the ongoing experiments (Condition E) at T-ADFA free-piston shock tunnel and these are listed in Table 1.

## 3. Convergence studies

In typical DSMC computations, it is critical to assign a proper distribution of cells over the domain to ascertain physically accurate selection of collision partners and also to estimate macroscopic flow properties from averaging the microscopic results. It is also important to have sufficient particle distribution over the domain so that the statistical errors can be minimized. In domains with significant flow gradients, it is therefore efficient to have a non-uniform cell distribution to minimize the spatial discretization errors. To achieve that, a flow based adaptation criterion is required so that the cell as well as particle distribution can be conveniently made in relation to the flow features. In the present simulations, a two pronged adaptation strategy is employed. To start with, a relatively coarse uniform grid of size within few orders of magnitude of the free-stream mean free path (mfp) is laid over the computational domain. The advantage of using a coarser initial grid is that the refinement can then be confined only to regions with high gradients.

Table 1: Free-stream values at test condition E in T-ADFA

Free-stream parameters	Values
$V_{\infty}$ , m/s	2490.0
$n_{\infty}$ , $m^{-3}$	$1.3364 \times 10^{23}$
$\rho_{\infty}$ , $kg/m^3$	0.0064
$\lambda_{\infty}$ , m	$8.43 \times 10^{-6}$
$Kn_{\infty}^{exp-surf}$	0.00042
$T_{tr_{\infty}}$ and $T_{rot_{\infty}}$ , K	151.0
$T_{vib_{\infty}}$ , K	
Oxygen (O <sub>2</sub> )	1220.0
Nitrogen (N <sub>2</sub> )	2500.0
Nitric Oxide (NO)	404.0
Mole fractions	
Oxygen (O <sub>2</sub> )	0.188
Nitrogen (N <sub>2</sub> )	0.766
Atomic Oxygen (O)	0.001
Nitric Oxide (NO)	0.045
Atomic Nitrogen (N)	0.000

However, a point to note here is that the initial coarse grid cannot be too large as otherwise many levels of refinement would be required to bring down the cell sizes around regions where the flow gradients are large (for eg. shocks). Here, the initial uniform cell size used is approximately  $5\lambda_{\infty}$ .

Once the model is read into the computational domain, a close surface clustering is done by refining cells close to the surface by a factor of 3. Thereafter, the simulation is run for 0.25ms, which corresponds to 5 flow lengths' time, so as to achieve a quasi-steady state in the domain. The macroscopic cell properties are calculated at this stage and a local cell-based mfp is estimated, which is a function of the local translational temperature. The ratio of the local mfp to the local cell size gives a local flow based Knudsen number ( $Kn_{loc}$ ). Ideally,  $Kn_{loc}$  should be greater than 1 everywhere so as to maintain the cell size within the range of local mfp. Physically, this is required as the collision partners are selected from within the same collision cell. Also, the flow gradient length scale are of the order of local mfp, so that the averaging of the microscopic particle properties should be done within this scale to resolve the macroscopic gradients. Hence, further refinement is carried out for cells less with  $Kn_{loc} < 1$ .

The final grid after all adaptations are run up to a total of 1ms, with the sampling of flow properties done at every 0.25ms interval. Such a large sampling interval, with running averages extending over to the previous sampling intervals (i.e. the average of the current sampling interval is in fact the cumulative average of the current and previous sampling intervals) reduces the statistical fluctuations in the result. With the fixed adaption procedure, the cell sizes and number of particles are progressively increased to check the relative level of convergence in the results. The various grid cases evaluated are presented in Table 2 and the separation lengths of both primary re-circulation region and secondary vortex, at the corner, are shown in Fig 2.

Table 2: Computed grid cases

Cases	Particles (in M)	Cells (in M)
1	111	4
2	107	7
3	105	13
4	104	20
5	207	20
6	206	30
7 <sup>a</sup>	135	29
8 <sup>a,BC</sup>	203	29

<sup>a</sup>Non-uniform refinement with one division more in Y direction; <sup>BC</sup>Best case

As far as the primary re-circulation region is concerned, the separation and re-attachment locations are reasonable resolved within 2% deviation from case 3 onwards. However, the secondary vortex at the corner shows a very unstable

## LEADING-EDGE SEPARATION

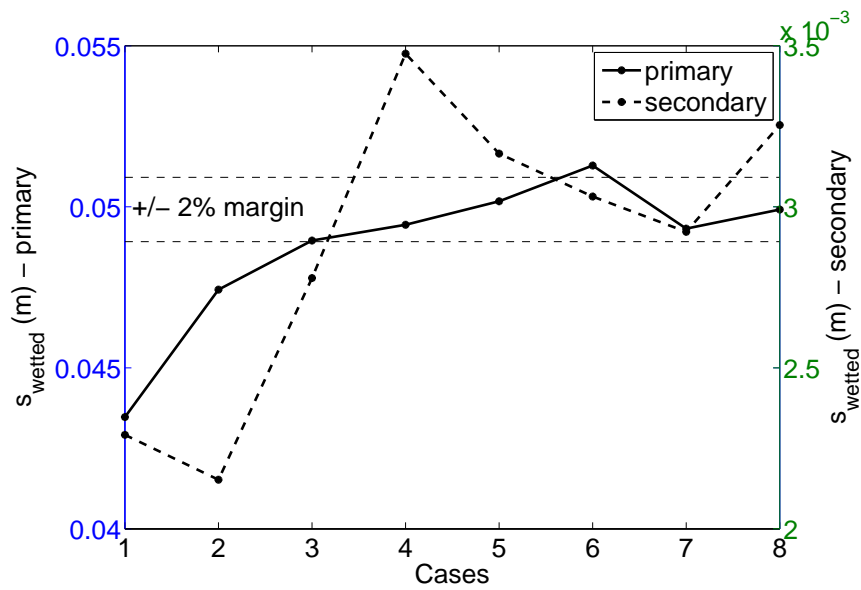
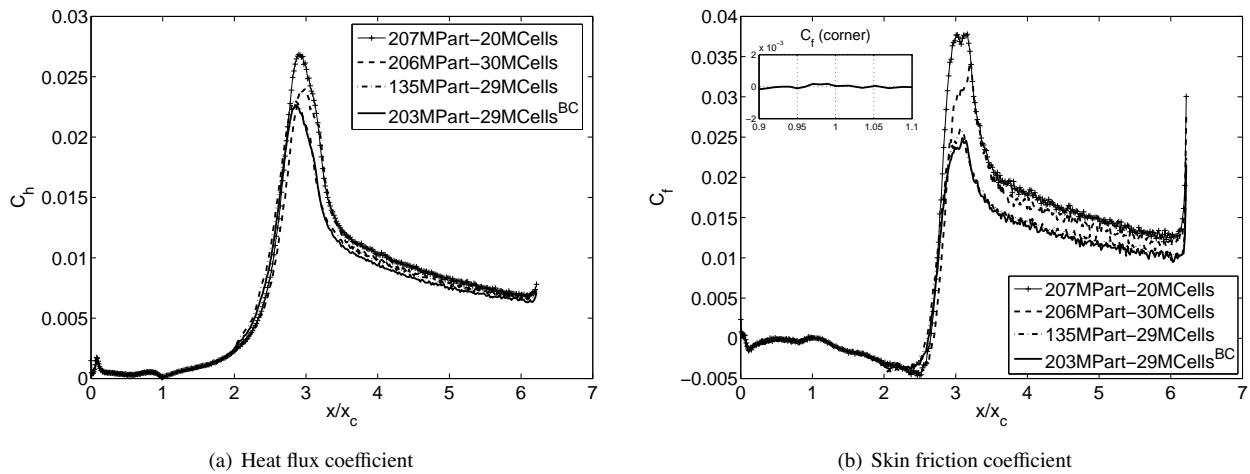


Figure 2: Separation lengths of primary and secondary re-circulation regions

behavior and this is to be expected for a bubble of this size. In order to further check the convergence, the distribution of heat flux and skin friction over the model for cases 5-8 (other cases are omitted for sake of clarity) are shown in Fig 3.

Figure 3:  $C_h$ - $C_f$  convergence for the computed grid cases

As shown in Fig 3, the deviations are observed mainly at the peaks of surface quantities and after the peak location. The skin friction is shown to be relatively more sensitive over the compression surface. Also, there is a slight shift of the peak locations among the compared cases in both the plots. An important observation is that the influence of particles are not as significant as that of the number of cells. This is noticeable when the best case (case 8) is compared with case 7. Though there is an increase of 68M in the total number of particles, the results don't vary much. This is due to the same number of cells and refinement structure used in both the cases. Having stated the importance of cell distribution, it is also equally crucial that every cell should contain on average a reasonable number of particles, called particles-per-cell (PPC). Otherwise, statistical fluctuations arise in the results. So, when the cells are refined to such an extent that the PPC gets lower, then either the sampling size should be increased or the total number of particles in the domain should also be correspondingly increased. The later approach is not always feasible when resources are limited as the computational requirement is directly linked to the total number of particles in the domain. In the present convergence studies, a balanced approach is followed to obtain the best case with the right combination of total particles and cells using the available resources. The best case simulation, obtained using 480 processors of

the National Computing Infrastructure's (NCI) Raijin cluster, took approximately 16 computational hours for every 0.25ms run.

The magnitude of peaks of surface quantities and corresponding locations, for all the cases considered, are shown in Fig 4. For both quantities, the peak magnitudes have been brought down within a deviation of 2% for the last two cases (case 7 and 8). The locations of the peak are relatively harder to resolve accurately as the re-attachment process is unsteady.

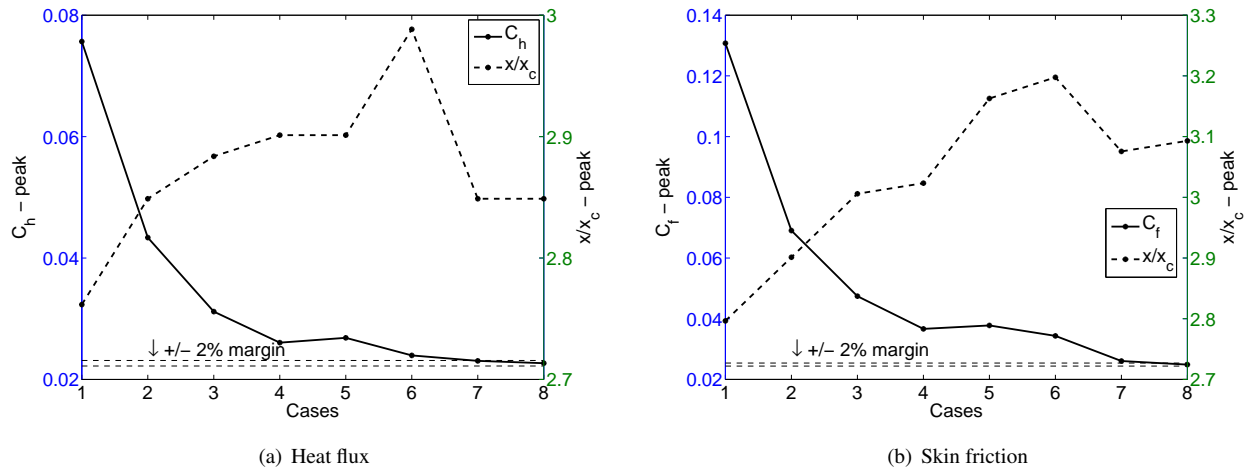


Figure 4: Convergence of peak values

### 3.1 Comparison with SMILE

To ascertain the accuracy of the best case obtained, the results are compared with high fidelity computations performed by Tumuklu et al<sup>12</sup> for the same model but using a different DSMC tool, called SMILE. In their work, they have used around 61M collision cells and 1.1B simulated particles. A web-based graph extractor is used to list out the values at 1.2ms from their plots to compare with the best case from SPARTA. The comparison is shown in Fig 5.

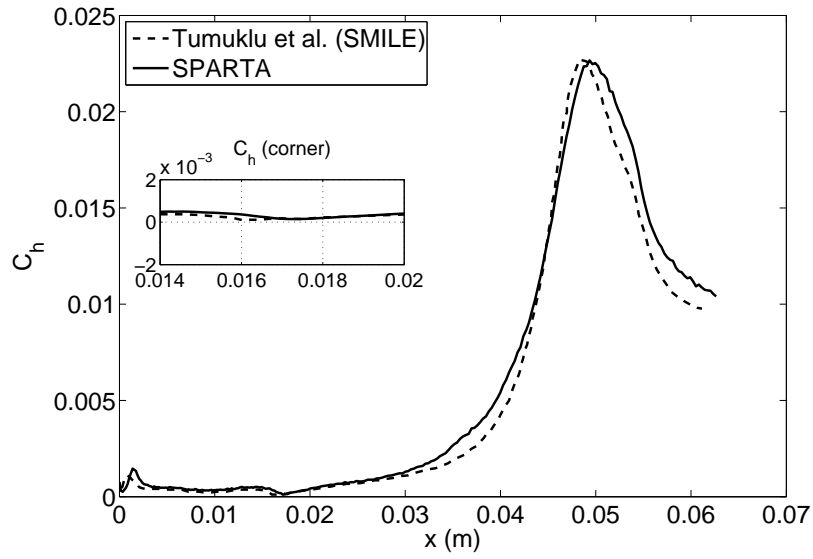
Both heat flux and skin friction coefficients show excellent agreement up to the peak, apart from a slight shift in locations of the respective peaks. Thereafter, the skin friction agrees well but the heat flux keeps a constant shift. For the velocity slip, the overall agreement is good but there are some discrepancies after the re-attachment peak and also for a small region between 0.02-0.03m, relative to the leading edge, on the compression surface. This region coincides with the location where the high vorticity close to the wall generated by the primary reverse flow shifts away and reduces in strength due to the presence of a secondary vortex at the corner. So, this region can be highly sensitive to the local cell sizes. The discrepancy after re-attachment can be possibly due to both the cell size and also the method by which  $V_{slip}$  is calculated for the best case. A direct computation of  $V_{slip}$  is not yet implemented in SPARTA so an interpolative approach is chosen. The velocities in global directions are transformed into surface parallel coordinates, separately for expansion and compression surfaces. Then, a line is drawn parallel to the surfaces, shifted by a constant distance of 1/3rd of the free-stream mfp ( $\lambda_{\infty}$ ). The transformed velocities in the cells through which the line passes are interpolated as  $V_{slip}$  values. As the flow regions after re-attachment are highly compressed between the surface and re-compression shock, the cell sizes can be relatively smaller due to the  $Kn_{loc}$  based adaptation. Therefore, the arbitrarily chosen line may not be passing through the first cell close to the surface.

## 4. Sharp leading edge geometry

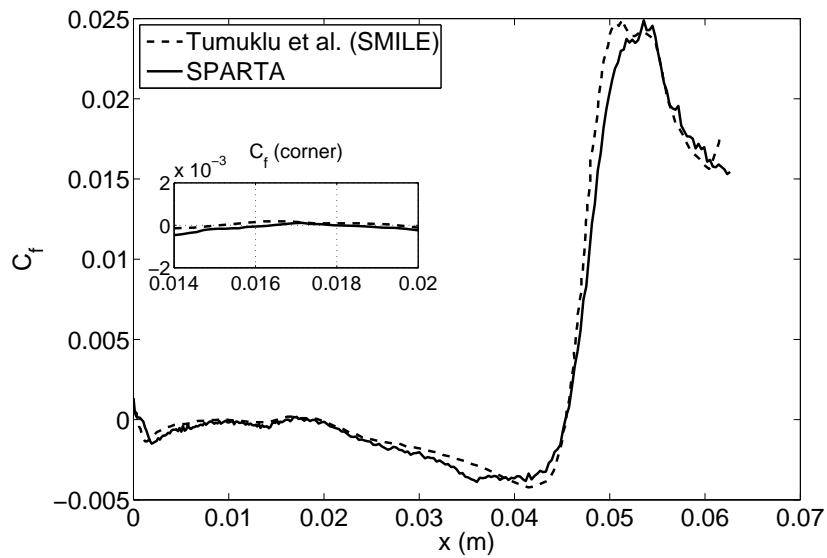
The best case from the previous section is run hereafter and results are evaluated in the sampling interval 1-1.25ms. The surface parameters are shown in Fig 6.

The pressure distribution displays the characteristic feature of a well-separated flow, which is a pressure plateau. The plateau extends till the corner and thereafter rises to the peak pressure just after re-attachment. The flow separation occurs at  $x/x_c = 0.045$ , based on  $V_{slip}$  and skin friction. This is consistent with the start of pressure rise at  $x/x_c = 0.01$ , the beginning of interaction, and the plateau is reached at approximately  $x/x_c = 0.21$ . After re-attachment, a characteristic feature of hypersonic flows is observed. There is a dip in pressure from the peak value, before retaining a constant inviscid pressure further downstream. This is due to the strength of the leading edge shock that interacts with

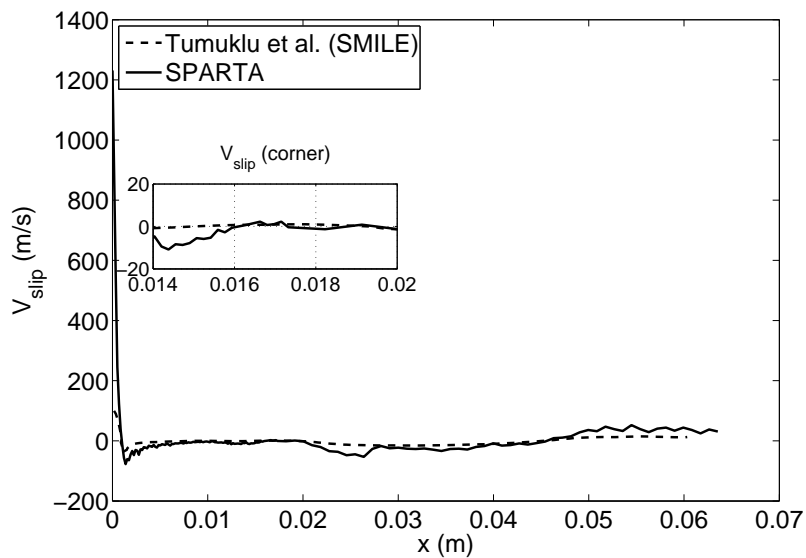
## LEADING-EDGE SEPARATION



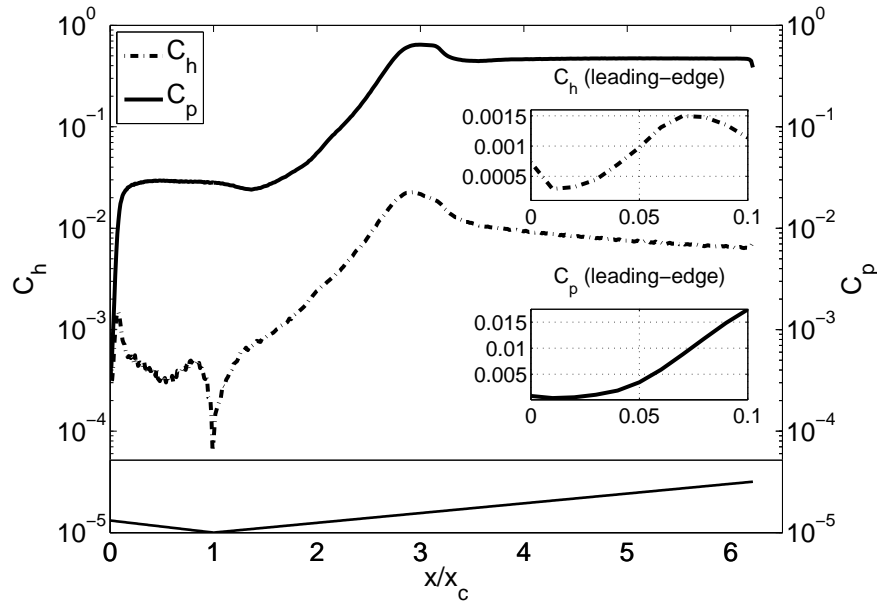
(a) Heat flux



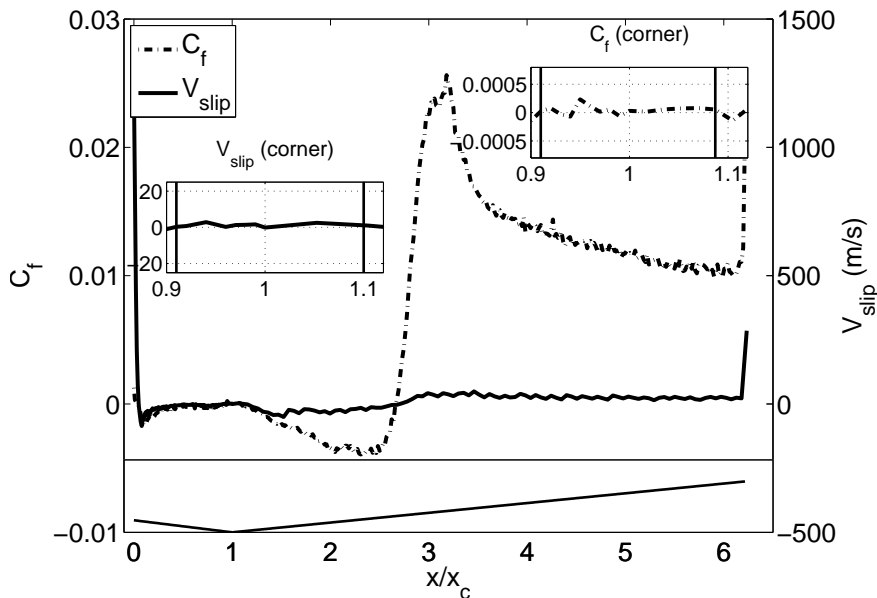
(b) Skin friction



(c) Velocity slip



(a) Heat flux and pressure coefficients



(b) Skin friction coefficient and velocity slip

Figure 6: Surface parameters - Sharp leading edge

the re-compression shock at the triple point, resulting in emanating expansion waves that hit the compression surface (see Fig 1). These expansion waves cause the dip in pressure. In supersonic flows, the leading edge shock may not be strong enough and dissipates faster. Hence, such a dip is generally not seen.

The heat flux first reduces rapidly along the surface after the leading edge before starting to rise again at the beginning of interaction (see inset of Fig 6a). The rise continues even after the separation location and terminates at a local maximum at  $x/x_c = 0.07$ . A possible reason for the presence of a local maximum in heat flux immediately after separation could be the slip effects in the flow. There is significant amount of slip along the surface till separation due to the strong expansion at the leading-edge. This is evident in the  $V_{slip}$  plot. The slipping of molecules is slowed down due to the adverse pressure gradient and has to dissipate as heat as the separation location is approached, resulting in a local rise in the heat flux as seen in the insets of Fig 6a. Thereafter, it exhibits a rounded profile up to  $x/x_c = 0.78$ , before sharply decreasing as the corner is approached. After the corner, it rises to the peak value at  $x/x_c = 2.936$ , which occurs just after re-attachment. After the peak, there is a sharp reduction due to expansion waves. It is then followed by a steady decrease along the compression surface, which is indicative of a developing boundary layer.

## LEADING-EDGE SEPARATION

The skin friction reduces from the leading edge, as the boundary layer starts to develop, and goes to zero at the separation location at  $x/x_c = 0.045$ . It stays negative along the expansion surface after separation due to the reverse flow in the re-circulation region. Close to the corner, it changes sign and goes above zero at the expansion surface and again goes below zero on the compression side (as shown as insets in Fig 6b). This indicates the presence of a small secondary vortex at the corner. The re-attachment occurs at  $x/x_c = 2.657$  and the skin friction rises to a sharp peak at  $x/x_c = 3.18$ . The reduction after peak is more drastic in the skin friction, relative to pressure and heat flux, and then comes to a steady decrease along the compression surface, which is due to the gradual velocity gradient reduction along a developing boundary layer.

Apart from the small region between the leading-edge and separation location, there is no significant presence of slip. However, the sign changes associated with flow reversals in both the primary and secondary vortex structures are well-captured in the  $V_{slip}$  distribution as well. Both skin friction and velocity slip agree on the separation and re-attachment locations of the primary re-circulation region and the secondary vortex, as seen in the insets of Fig 6b.

In Tumuklu et al,<sup>12</sup> it has been found that the secondary vortex develops over the time and enlarges to a sizable vortex structure. This vortex then stretches out from approximately half way through the expansion surface and all the way to the corner, engulfing the corner vortex. They also pointed out that this enlargement of secondary vortex is a slow development and the final result presented for 2.6ms was still found to be developing. At 1.2ms, there was no sign of any large asymmetric secondary vortex, apart from a small Moffat type eddie at the corner. In order to corroborate this, the present case is run longer up to 2.25ms. The streamline pattern from the present case at times of 1.2ms and 2.25ms are shown in Fig 7.

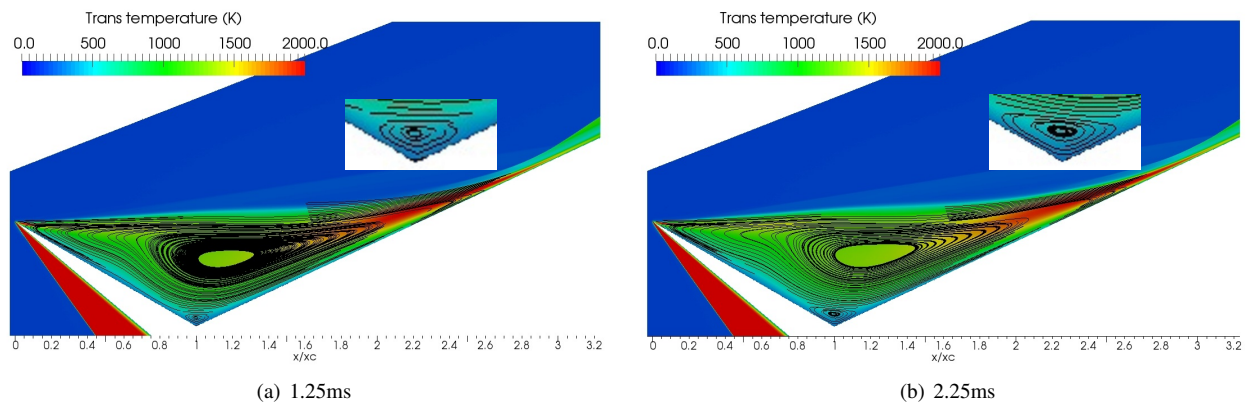


Figure 7: Streamline pattern

In Fig 7, there are no signs of a sizable secondary vortex. However, at 2.25ms, the corner eddie seems slightly enlarged and stretched out more onto the expansion surface. The only plausible way in the present flow condition for the corner vortex to develop, within the primary structure, is by draining energy from the primary vortex. Such an energy transfer can happen only through vorticity generated either by viscous interaction close to the wall or through turbulence. The later can be discarded as we are dealing with a fully laminar flow. It is, therefore, worthwhile to check the vorticity distribution over the flow field at 1.25ms.

As shown in Fig 8, there is a region of high vorticity close to the compression wall generated by the reverse flow stream of the primary vortex. This starts at the re-attachment and proceeds towards the corner. The corner vortex would then be fed with energy from this jet of reverse flow, resulting in stretching it out towards the expansion side. Close to the separation location, another high vorticity region is evident that extends up to  $x/x_c = 0.4$ . This vorticity is responsible for the bending of streamlines away from the wall as seen in the streamline patterns in Fig 7. In course of time, these two mechanisms would merge and form a single larger secondary vortex, as shown in Tumuklu et al.<sup>12</sup>

Now, the question arises as to the absence of such a large secondary vortex in the present case even after running it up to 2.25ms. A possible reason for this discrepancy, relative to the results of Tumuklu et al,<sup>12</sup> could be the grid inadequacy. As presented in the convergence studies, the best case grid structure is generated on the basis of quasi-steady flow conditions obtained at around 0.25ms. Within that time, only the primary structure is fully developed and a Moffat eddie at the corner. Since a flow based adaptation criterion ( $Kn_{loc}$  based) is chosen, all the features that develop in such a short time are well captured. However, the secondary vortex starts to develop only after 1.5ms and still shows a developing behavior at 2.25ms. In the present case, no adaptations are carried out after 0.25ms so the grid may not be adequate to capture such later developments. A possible solution would be to further adapt the grid, using the same criterion, either continuously for every sampling interval or start with a further refined grid. These options are presently being explored.

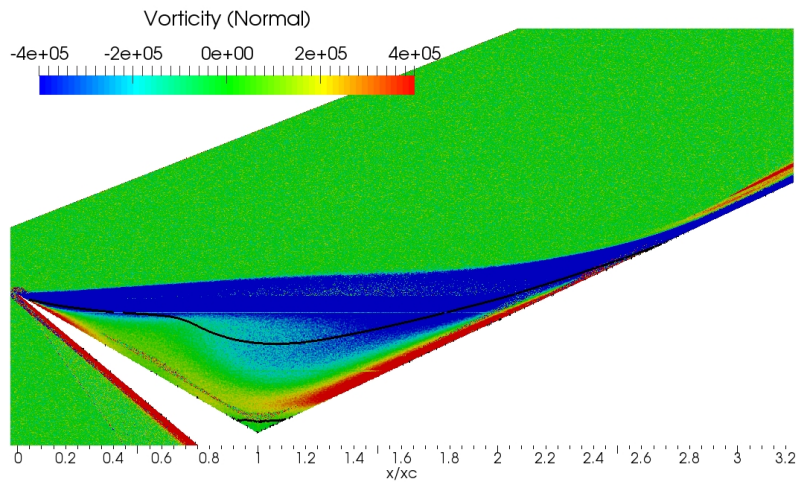


Figure 8: Vorticity distribution at 1.25ms (Zero X velocity contours are included)

## 5. Theoretical analysis of separation and re-attachment streamlines

The behavior of streamlines at separation in a general laminar incompressible or compressible flow, with or without heat conduction, was first theoretically proposed by Oswatitsch<sup>13</sup> through a local analysis of the Navier-Stokes (NS) equations, which for the 2D flow is:

$$\tan \theta_S = -3 \left( \frac{d\tau_w/dx}{dp_w/dx} \right)_S \quad (1)$$

where  $\theta_S$  is the angle of the separation streamline,  $\tau_w$  the wall shear stress,  $p_w$  the wall pressure and  $x$  the stream-wise length. The subscript  $S$  denotes the values evaluated at the location of separation.

This expression is also applicable to the streamline angle at re-attachment. In order to check the validity of the criterion in the present case, the angle of streamline at separation and re-attachment locations is first determined. It is tedious to calculate the correct angles based on streamline behavior as the slopes can be quite sensitive close to the separation and re-attachment locations. To minimize the error introduced as a result of image based angular determination, a contour is drawn along which the global stream-wise velocity component goes to zero. This clearly identifies the separation and re-attachment locations, which should closely match with the predictions from skin friction and velocity slip distribution. The separation streamline has its origin on the separation location but has a slope larger than the zero velocity contour line. So a tangent line is drawn from the separation point to the separation streamline to determine the angle of separation. A similar approach is used at the re-attachment location as well to determine the angle of re-attachment ( $\theta_R$ ). The measured angles from streamlines, along with the zero velocity contour angles ( $\theta_{ZV}$ ), are shown in Figures 9 and 10.

The characteristics of skin friction and pressure at separation and re-attachment locations are shown in Figure 11, from which the theoretical slopes can now be determined. The magnitude of the slopes thus estimated are marked in the figure. The comparison between the measured angles based on streamline behavior and the theoretical slopes of stream-wise pressure and skin friction gradients are given in Table 3. It was shown by Oswatitsch<sup>13</sup> that slope of the curve of vanishing stream-wise velocity component, which is the contour of zero X velocity (ZV) in Figures 9 and 10, is 2/3rd of the separation streamline slope.

At the re-attachment location, the angles show good agreement but it is not the case at the separation location. The reason for this disagreement is the significant slip effects in the flow that occurs till the flow separates. Due to the expansion at the leading edge, the flow gets rarefied with inherent slip effects on the wall. The slip effect increases the slope of the streamlines leaving the wall due to higher velocities within the Knudsen layer. The original slip equation relating the tangential gas velocity slip to shear stress and heat flux, as proposed by Maxwell,<sup>15</sup> can be written in the 2D form as

## LEADING-EDGE SEPARATION

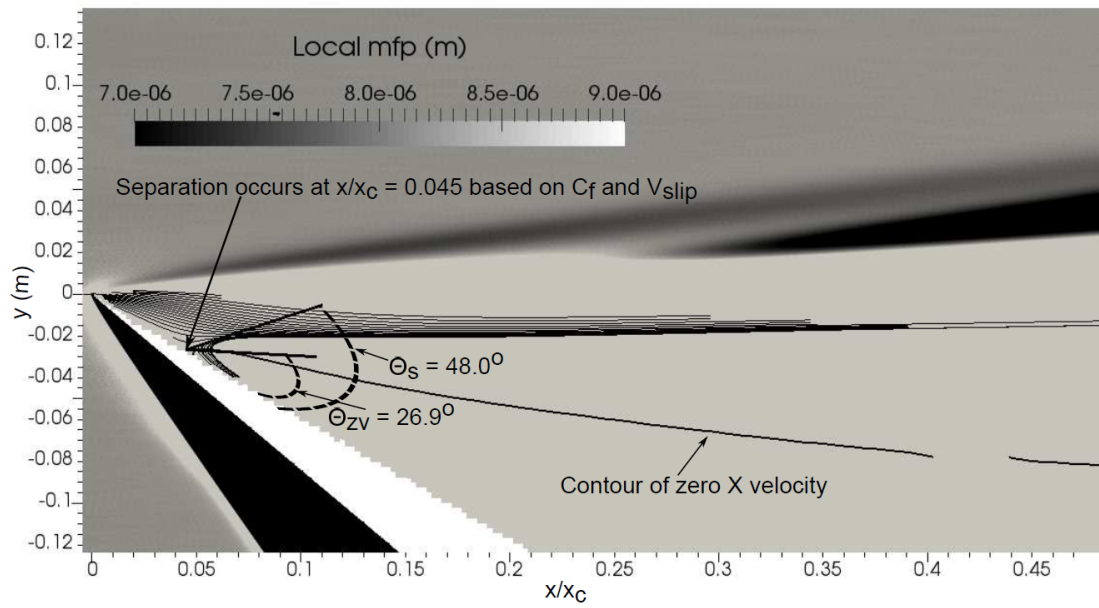


Figure 9: Streamline angle at separation

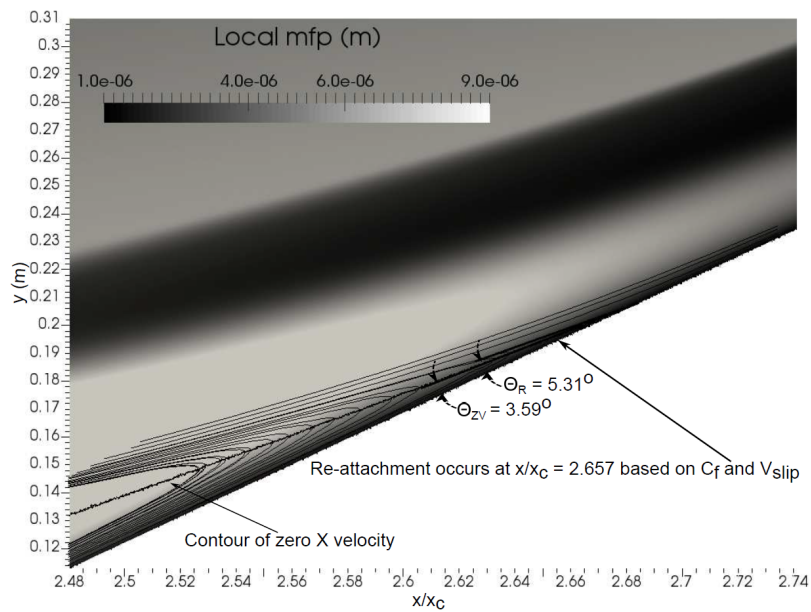


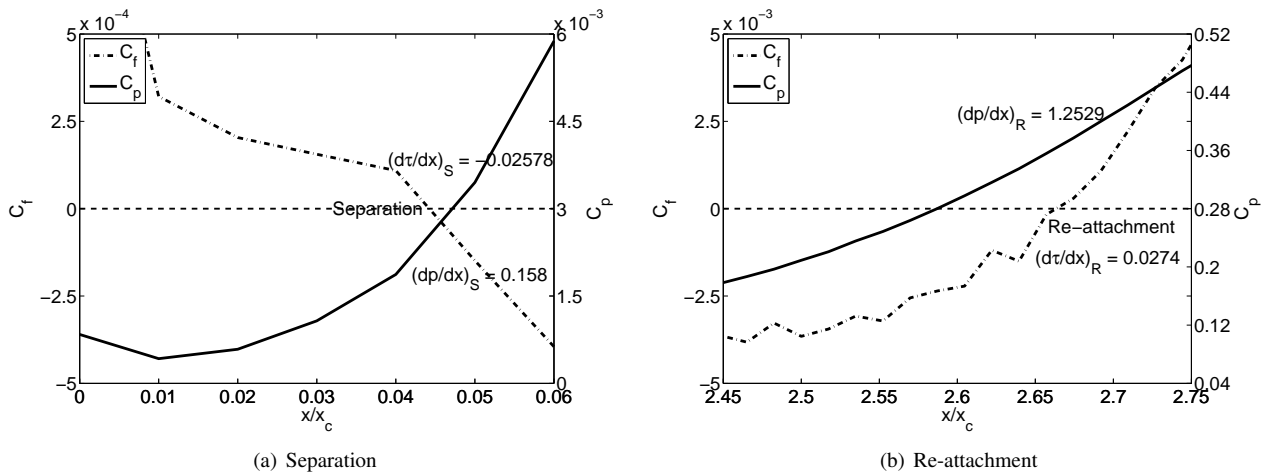
Figure 10: Streamline angle at re-attachment

Table 3: Comparison between streamline and theoretical separation/re-attachment angles

	Streamline	Theory <sup>a</sup>
$\theta_S$	48.0°	26.08°
$\theta_{ZV-S}$	26.9°	32.0°
$\theta_R$	5.31°	3.75°
$\theta_{ZV-R}$	3.59°	3.54°

<sup>a</sup>Based on numerical prediction of gradients in Eq.1

$$u_{slip} = \lambda_{gw} \left( \frac{\partial u}{\partial y} + \frac{\partial v}{\partial x} \right) + \frac{3}{4} \frac{\mu_{gw}}{\rho_{gw} T_{gw}} \frac{\partial T_{gw}}{\partial x} \quad (2)$$

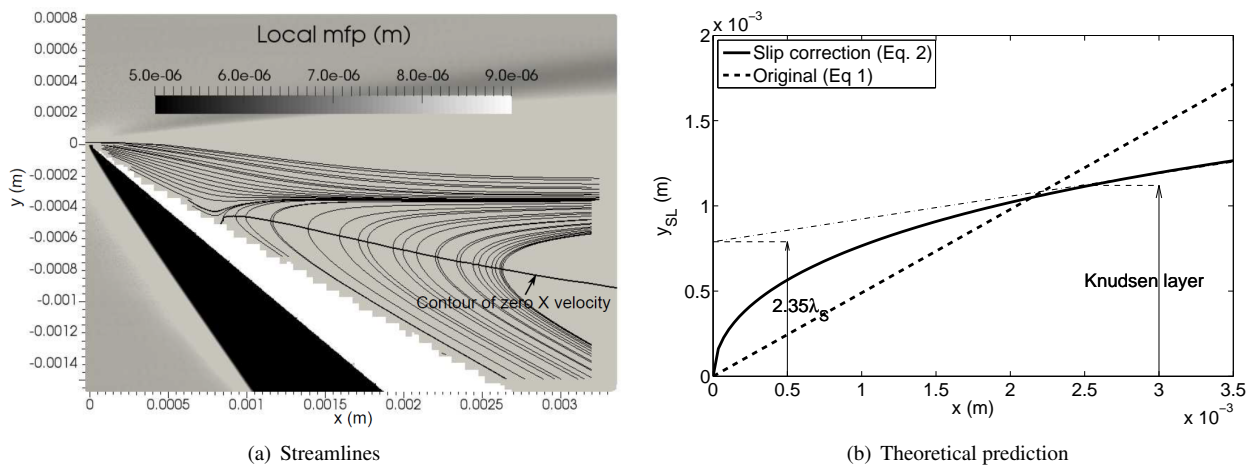
Figure 11:  $C_f$ - $C_p$  profiles close to separation and re-attachment

where  $u, v$  are the wall stream-wise and normal velocity components,  $\lambda$  the mean free path,  $\mu$  the viscosity,  $\rho$  the density and  $T$  the temperature. The subscript  $gw$  denotes the values of gas at the wall.

Inger and Moss<sup>16</sup> proposed a correction to take into account the influence of slip effects on the separation angle by including a slip correction term to Eq.1. For that, they used a reduced form of Eq. 2, where only the first term on the right hand side is considered. Such a reduction pose limitations due to geometry and non-equilibrium in the flow. When the geometry is curved, stream-wise gradient of the normal velocity ( $\partial v/\partial x$ ) can be substantial enough to influence the slip. Similarly, a strongly expanded flow moving against an adverse pressure gradient can have significant temperature gradients in the stream-wise direction ( $\partial T/\partial x$ ). In the present case, the incoming flow is bent parallel to the expansion surface at the leading edge and undergoes separation within 1mm. This would induce some contributions from the omitted terms. However, it is worthwhile to check the separation streamline profile with that of the theoretical correction of Inger and Moss,<sup>16</sup> which has the following form

$$x \tan \theta_{S0} = \frac{(1 - C_1 \lambda_{gw_s}) y_{SL}^2}{2 \lambda_{gw_s} + (1 - C_2 \lambda_{gw_s}) y_{SL}} \quad (3)$$

where  $C_1 = \left( \frac{dp_w/dx}{p_w} \right)_s$  and  $C_2 = \left( \frac{dT_{gw}/dy}{T_{gw}} \right)_s$ . The subscript  $s$  denotes that the values are taken at the separation location, as in Eq.1, and  $y_{SL}$  is the streamline profile at the separation location.  $\theta_{s0}$  is the no-slip value of streamline angle from Eq.1, and using this the profile shape can be determined by solving Eq. 3. The theoretical no-slip and slip corrected profiles are shown in Fig 12, along with the numerically predicted streamline profile at separation.

Figure 12: Numerical and theoretical streamline profiles at separation ( $\lambda_{gw_s} = 0.336\text{mm}$ )

As shown in Fig 12a, the streamlines from computations show a wall normal behavior close to the wall. The

## LEADING-EDGE SEPARATION

theoretical profile in Fig 12b shows a normal slope close to the wall and turns into a highly curved region within a wall normal distance corresponding to  $2\lambda_{gws}$ , before evolving into a linear behavior further away. The original relation of Oswatitsch shows a constant slope at the wall, which is characteristic of a no-slip flow based on which that relation is derived. The slip correction takes into account of the tangential velocity changes occurring within the Knudsen layer and hence captures the slope changes more effectively, which is evident in the theoretical prediction in Fig 12b.

## 6. Conclusions

A leading-edge separation model, subjected to hypersonic flow conditions, is computationally studied to assess separation and re-attachment characteristics. A flow based grid adaption method is chosen to generate a grid distribution that can properly resolve the local flow gradients. A close-surface clustering in combination with local Knudsen number ( $Kn_{loc}$ ) based grid adaptation gives a reasonable distribution that resolves the flow features efficiently. Such adaptation methods are important especially when the computational resources are limited. The convergence of the best case obtained is evaluated in terms of both the separation length and peak value of surface parameters. Further, the result obtained at 1.25ms shows reasonable agreement with high fidelity computations done by Tumuklu et al.<sup>12</sup> One limitation while using a flow based adaptation is that unless the adaptation is done continuously any significant flow developments occurring after the adaptation procedures may not be well resolved. However, a continuous adaptation is not always desirable as it may result in many levels of refinements that pose limitations on the bit based hierarchical grid id allocation in SPARTA. A way to avoid this problem would be to set the adaptation to occur at limited number of predetermined intervals. In many situations, apriori knowledge regarding the timescales of secondary developments in the flow-field is not known so it is not straightforward to set the adaptation intervals. To overcome this, as DSMC is inherently transient, the time history of results can be evaluated and the unsteadiness in the flow-field is determined. This would help in setting up proper intervals at which adaptation procedures need to be repeated.

The pressure distribution over the sharp leading-edge model shows the characteristics of a well-separated flow. The heat flux shows a strong reduction after the leading edge due to slip effects and then starts to rise at the beginning of interaction. It rises to a local maximum after separation. This is possibly a characteristic of slip flows.

The skin friction and velocity slip clearly identify both separation and re-attachment locations of the primary vortex. Though the flow is predominantly in the continuum regime, there is a significant amount of slip in the region between the leading edge and separation. The velocity slip stays close to zero everywhere else. At the corner, the secondary vortex is found to exist though not well resolved. Both skin friction and velocity slip show sign changes at the secondary vortex location. The secondary vortex at 1.25ms is similar to that found by Tumuklu et al. However, due to limitations of the present grid, the secondary structure is not properly resolved for the present case even at 2.25ms.

The theoretical analysis of streamline angles at separation show good agreement with the slip corrected relation of Inger and Moss. It is observed that slip makes the separation streamline leave the wall with a normal slope before turning into a highly curved region within the Knudsen layer. At the re-attachment, the streamline angle is predicted reasonably well by the Oswatitsch relation.

## Acknowledgments

This study forms part of the Australian Research Council Grant, DP-140100842, and this support is gratefully acknowledged. We would like to acknowledge that this research was undertaken with the assistance of resources and services from the National Computational Infrastructure (NCI), which is supported by the Australian Government. Also, we would like to thank Dr. Michael Gallis, who is one of the developers of SPARTA code at Sandia National Laboratories, for his helpful advice.

## References

- [1] Chapman, D., Kuehn, D., and Larson, H., "Investigation of Separated Flows in Supersonic and Subsonic Streams with Emphasis on the Effect of Transition," NACA Technical Report 1356, 1958.
- [2] Holden, M., "A Study of Flow Separation in Regions of Shock Wave-Boundary Layer Interaction in Hypersonic Flow," *11th Fluid and Plasma Dynamics Conference*, No. 1169, AIAA, Jul. 1978.
- [3] Deepak, N., Gai, S., and Neely, A., "High-Enthalpy Flow over a Rearward-Facing Step - A Computational Study," *Journal of Fluid Mechanics*, Vol. 695, Mar. 2012, pp. 405–438.

- [4] Harvey, J., Holden, M., and Wadhams, T., "Code Validation Study of Laminar Shock/Boundary Layer and Shock/Shock Interactions in Hypersonic Flow Part B: Comparison with Navier-Stokes and DSMC Solutions," *39th Aerospace Sciences Meeting and Exhibit*, No. 1031, AIAA, 2001.
- [5] Moss, J., O'Byrne, S., Deepak, N., and Gai, S., "Simulations of Hypersonic, High-Enthalpy Separated Flow over a 'Tick' Configuration," *28th International Symposium on Rarefied Gas Dynamics*, No. 1501, Jul. 2012, pp. 1453–1460.
- [6] Moss, J., O'Byrne, S., and Gai, S., "Hypersonic Separated Flows about "Tick" Configurations with Sensitivity to Model Design," *AIP Conference Proceedings*, No. 1628, Jul. 2014, pp. 162–169.
- [7] Bird, G. A., *The DSMC method*, CreateSpace Independent Publishing Platform, 2013.
- [8] Prakash, R., Gai, S., and O'Byrne, S., "Numerical Study of Hypersonic Separated Flow over an Expansion-Compression Surface," *20th AIAA International Space Planes and Hypersonic Systems and Technologies Conference*, No. 3528, Jul. 2015.
- [9] Prakash, R., Gai, S., O'Byrne, S., and Brown, M., "DSMC Computations of Hypersonic Flow Separation and Re-attachment in the Transition to Continuum Regime," *AIP Conference Proceedings*, No. 1786, Nov. 2016.
- [10] Prakash, R., Gai, S., and O'Byrne, S., "DSMC Computations of Separation over a 'Tick' model in Hypersonic High Enthalpy Transitional Flows," *55th AIAA Aerospace Sciences Meeting, AIAA SciTech Forum*, No. 1844, Jan. 2017.
- [11] O'Byrne, S., Kaseman, T., Krishna, Y., Gai, S., Kleine, H. H., and Neely, A., "Leading-Edge Separation in Thermal Nonequilibrium Hypersonic Flow Final Report for AOARD Grant 134013," SEIT, UNSW-ADFA Grant Report, 2014.
- [12] Tumuklu, O., Levin, D., and Theofilis, V., "On the Temporal Evolution in Laminar Separated Boundary Layer Shock-Interaction Flows using DSMC," *55th AIAA Aerospace Sciences Meeting, AIAA SciTech Forum*, No. 1614, Jan. 2017.
- [13] Oswatitsch, K., *Die Ablosungsbedingung vo Grenzschichten*, International Union of Theoretical and Applied Mechanics Symposium, Springer-Verlag, 1957, pp. 357–367.
- [14] Moffat, H. K., "Viscous and Resistive Eddies near a Sharp Corner," *Journal of Fluid Mechanics*, Vol. 18, No. 1, 1964, pp. 1–18.
- [15] Lockerby, D. A., Reese, J. M., Emerson, D. R., and Barber, R. W., "Velocity Boundary Condition at Solid Walls in Rarefied Gas Calculations," *Physical Review E*, Vol. 70, No. 017303, 2004.
- [16] Inger, G., "Scaling of Incipient Separation in High Speed Laminar Flows," *AIAA Journal*, Vol. 33, No. 1, 1995, pp. 178–181.